Bioorganic Chemistry 88 (2019) 102981

Contents lists available at ScienceDirect

Bioorganic Chemistry

journal homepage: www.elsevier.com/locate/bioorg

Investigation of the interaction between salvianolic acid C and xanthine oxidase: Insights from experimental studies merging with molecular docking methods

Hongjin Tang[a,*], Dongsheng Zhao[b]

[a] College of Biological and Chemical Engineering, Anhui Polytechnic University, Wuhu 241000, PR China
[b] College of Pharmacy, Shandong University of Traditional Chinese Medicine, Jinan 250355, PR China

ARTICLE INFO

Keywords:
Salvianolic acid C
Xanthine oxidase
Interaction mechanism
Molecular docking

ABSTRACT

Xanthine oxidase (XO) has emerged as an important target for gout. In our previous study, salvianolic acid C (SAC) was found to show potent XO inhibitory activity, whereas the interaction mechanism was still not clear. Herein, an integrated approach consisting of enzyme kinetics, multi-spectroscopic methods and molecular docking was employed to investigate the interaction between SAC and XO. Consequently, SAC exhibited a rapid and mixed-type inhibition of XO with IC_{50} of 5.84 ± 0.18 μM. The fluorescence data confirmed that SAC presented a strong fluorescence quenching effect through a static quenching procedure. The values of enthalpy change, entropy change and Gibbs free energy change indicated that their binding was spontaneous and driven mainly by hydrophobic interactions. Analysis of synchronous fluorescence, circular dichroism and fourier transform infrared spectra demonstrated that SAC induced conformational changes of the enzyme. Besides, further molecular docking revealed that SAC occupied the catalytic center resulting in the inhibition of XO activity. This study provides a comprehensive understanding on the interaction mechanism of SAC on XO.

1. Introduction

Gout is a common form of inflammatory arthritis characterized by recurrent acute attacks triggered by the precipitation of monosodium urate (MSU) crystals in joints, tendons, kidneys and surrounding tissues. The crystallization of uric acid is closely associated with an elevated uric acid level in blood, namely, hyperuricemia [1]. Persistent hyperuricemia has emerged as the most important pathologic factor of chronic gout. To date, two effective drug therapeutic strategies have been used to decrease serum uric acid level including inhibiting urate production and accelerating renal uric acid excretion, such as xanthine oxidase (XO) inhibitor and uricosuric. XO, a versatile molybdoflavoprotein, is specially distributed in liver and intestine of human [2,3]. XO is the critical and rate-limiting enzyme involving in uric acid biosynthesis in humans that catalyzes the oxidation of hypoxanthine to xanthine and follows to the final product uric acid, accompanied by the generation of reactive oxygen species (ROS), such as superoxide anions and hydrogen peroxide [4]. Excess ROS can interfere in cell functions and result in cellular damage, which is associated with various pathological progresses such as inflammation, cardiovascular diseases and even carcinoma [5]. Also, the overproduction of uric acid can cause hyperuricemia, gout and other related complications [6]. Therefore, XO has been considered as one of the most promising targets for controlling uric acid levels and treating hyperuricemia and gout [7]. Allopurinol (Fig. 1), a prototype XO inhibitor, has been used as anti-gout drug in clinic for several decades due to obvious curative effects [8]. Febuxostat (Fig. 1, approved in USA, 2009), a non-purine XO inhibitor, has already been developed as the most widely prescribed therapeutic drug for the management of hyperuricemia and chronic gout worldwide [9]. However, they are still restrained from their clinical applications because of serious adverse effects, such as progressive renal failure, fulminant hepatitis and Steven-Johnson syndrome [10]. Under these limitations, there is an increasing demand to develop novel XO inhibitors with more potent XO inhibitory activity and fewer side effects for the treatment of gout and its complications.

Recently, large amounts of excellent XO inhibitors with various chemotypes have been reported, such as topiroxostat [11], Y-700 [12], selenazoles [13] and imidazoles [14] (Fig. 1). Natural products have always played an important role in developing drug leads [15–17] and a variety of potent XO inhibitors have been isolated from natural products, such as curcumin, hyprhombin C, hydroxychavicol and neotaiwanensol B [18–20]. From the view of pharmacology, accurate

* Corresponding author.
E-mail address: tanghongjin@ahpu.edu.cn (H. Tang).

https://doi.org/10.1016/j.bioorg.2019.102981
Received 22 February 2019; Received in revised form 6 May 2019; Accepted 8 May 2019
Available online 09 May 2019

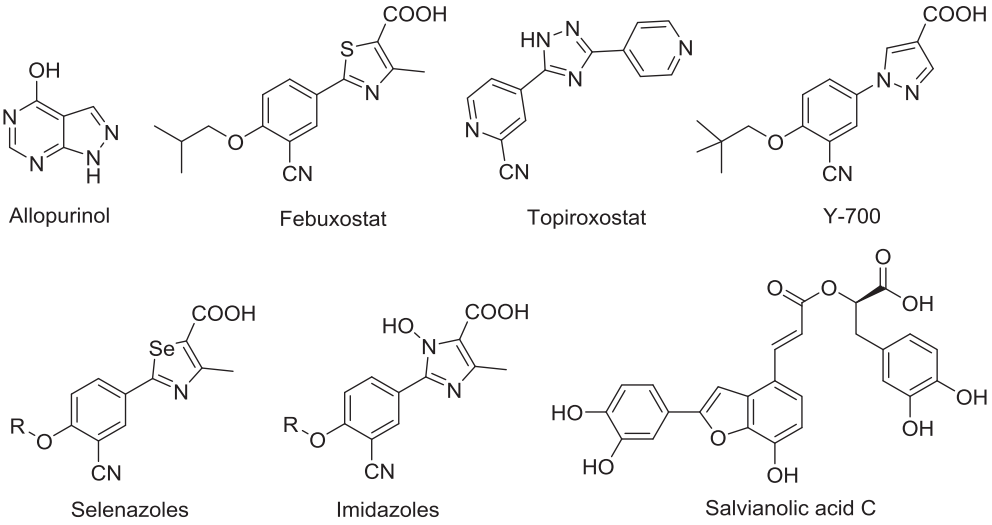

Fig. 1. The chemical structures of the well-known XO inhibitors.

comprehending of interaction mechanism between bioactive molecules and protein is of great importance, which may be due to that it can reflect the binding characteristic of proteins forming bonds with small molecules and help to develop new drugs in terms of a comprehensive understanding of their interaction relationships with body proteins. Thus, it is necessary for drug-protein system to perform the interaction studies between small molecules and proteins at the molecule level, which can provide valuable information in drug design, molecular recognition mechanism and chemical biology.

Currently, the development of many spectroscopic techniques, such as ultraviolet visible spectroscopy, fluorescence spectroscopy, dynamic light scattering, fourier transform infrared spectroscopy (FT-IR) and circular dichroism (CD) spectrum, makes great contribution to the discovery of drug candidates, which may be ascribed to their prominent advantages including time- and labor-saving, high sensitivity and reproducibility, convenience and so forth [21]. In recent years, such methods have been widely applied to clarify the binding behaviors and interaction mechanism of drug-protein system coupled with *in vitro* and *in vivo* experiments [22,23]. For example, Zhang et al. employed multi-spectroscopic methods to study the interaction between maltol (a food additive) and bovine serum albumin [22]. Furthermore, molecular modelling has also emerged as a common method to predict the proposed binding mechanism for active molecules and proteins [24].

The natural product salvianolic acid C (SAC) (Fig. 1) isolated from the traditional Chinese medicine *Salvia miltiorrhiza*, was found as a potent XO inhibitor and then a library of SAC derivatives was synthesized in our previous study [25]. However, the inhibition effect between SAC and XO was evaluated mainly based on the enzymatic assay and the detailed interaction behavior was still unknown. Thus, in the present study, multi-spectroscopic approaches were used to explore the interaction relationship between SAC and XO. The enzyme inhibition and inactivation kinetics, fluorescence quenching spectroscopy and molecular docking studies were employed to determine the inhibitory effect, binding mode and thermodynamic parameters. Simultaneously, the synchronous fluorescence, ANS-binding fluorescence, FT-IR and CD spectra were also performed to investigate the conformational changes of the enzyme mediated by SAC. This study may provide new insights into understanding the inhibition mechanism of SAC on this important enzyme, suggest some significant clues to the design of SAC-derived drug leads as new XO inhibitor and is beneficial to improve application of SAC derivatives as drug candidates in the prevention and treatment of hyperuricemia, gout and related complications.

2. Materials and methods

2.1. Chemicals and reagents

The reference standard SAC was purchased from the National Institute for the Control of Pharmaceutical and Biological Products (Beijing, China) (purity > 99%). XO (isolated from bovine milk, EC 1.17.3.2), 8-anilino-1-naphthalenesulfonate (ANS) and xanthine were obtained from Sigma-Aldrich Chemical Co. (USA). Allopurinol was purchased from Toronto (North York, Canada). All other reagents and solvents were of analytical reagent grade and ultrapure water was used throughout the experiment.

2.2. Apparatus

The enzyme kinetic assay was performed on a Thermo Multiskan Go v1.01.10 microplate spectrophotometer (USA). The fluorescence spectra were measured on a Hitachi F-7000 spectrofluorophotometer (Japan) with a 1.0 cm quartz cuvette. The thermostat water bath (Shanghai double shun industry development Co., LTD) was used to control the experimental temperature. The FT-IR spectra were recorded on a Shimadzu FT-IR Prestige-21 spectrometer (Japan) equipped with a germanium attenuated total reflection (ATR) accessory. CD spectra were measured on a JASCO-810-CD spectrometer (Japan) with a 1.0 mm path length quartz curette. All the experiments were conducted at room temperature unless specified otherwise.

2.3. Preparation of stock solutions

XO and xanthine were dissolved in 75 mM phosphate buffer solution (PB, pH 7.0) to prepare 10 U/mL and 50 mM of stock solutions, respectively. The fluorescence probe ANS was dissolved in absolute ethanol to obtain a 100 mM of stock solution. The stock solutions (100 mM) of compounds SAC and allopurinol were prepared by dissolving in DMSO respectively, and were diluted to the required concentration with PB. The contents of DMSO in each sample were less than 0.1%.

2.4. Evaluation of XO inhibitory activity in vitro

The XO inhibition activity experiment was completed according to the previous method with slight modifications [25]. In brief, various concentrations of SAC (100 μL) and fixed concentration of XO (50 μL, 0.08 U/mL) were equilibrated for 3 min at 37 °C. Subsequently, the

reaction was started by adding xanthine solution (50 μL, 0.48 mM). The absorbance of the mixture was recorded every 15 s for 7 min at 295 nm on a microplate spectrophotometer. The blank control was set without the test compound and allopurinol was used as the positive control. The inhibition ratio of compounds on XO is calculated by the Eq. (1):

$$Inhibition\ \ ratio\ \ (\%) = \frac{\left(\frac{dA}{dt}\right)_{blank} - \left(\frac{dA}{dt}\right)_{sample}}{\left(\frac{dA}{dt}\right)_{blank}} \times 100 \quad (1)$$

where $\left(\frac{dA}{dt}\right)_{blank}$ and $\left(\frac{dA}{dt}\right)_{sample}$ refer to the enzyme reaction rate of blank group and sample, respectively. The IC_{50} value representing the inhibitory strength of test compound against XO, was calculated using Excel 2013 and GraphPad v6.02.

2.5. Measurement of inhibition reversibility and inhibition type

Inhibition reversibility was determined by maintaining substrate concentration (0.12 mM) and increasing the concentration of XO (0.0125, 0.025, 0.05 and 0.1 U/mL). The reaction velocity (v, ΔA/min) was measured by adding various concentrations of SAC (0, 1.25, 2.5, 5, 10 and 25 μM). The assay was taken according to the method of 2.4. Then inhibition reversibility of SAC on XO was concluded by plotting the reaction velocity and enzyme concentration.

Inhibition type was measured by maintaining the final concentration of XO (0.02 U/mL) and changing xanthine concentration from 50 to 200 μM. The reaction velocity was measured by adding varied concentrations of SAC. The double reciprocal Lineweaver-Burk plots were depicted to determine the kinetic mechanism of XO inhibited by SAC through the Eq. (2) [26].

$$\frac{1}{v} = \frac{K_m}{V_m}\left(1 + \frac{[I]}{K_i}\right)\frac{1}{[S]} + \frac{1}{V_m}\left(1 + \frac{[I]}{\alpha K_i}\right) \quad (2)$$

K_i and K_{is} are the inhibition constants of compound binding with the free enzyme and enzyme substrate complex respectively, which can be obtained from the secondary plots of Lineweaver-Burk curves as the Eqs. (3) and (4):

$$\text{Slope} = \frac{K_m}{V_m} + \frac{K_m[I]}{V_m K_i} \quad (3)$$

$$Y - intercept = \frac{1}{V_m^{app}} = \frac{1}{V_m} + \frac{[I]}{\alpha K_i V_m} \quad (4)$$

where v is the enzyme reaction rate with or without flavonoids and K_m is the Michaelis-Menten constant. α is the ratio of the uncompetitive inhibition constant to competitive inhibition constant. If the value of α is 1, it belongs to a noncompetitive inhibition. [I] and [S] are the concentrations of inhibitor and substrate, respectively. The secondary plots of slope versus [I] are linearly fitted, assuming a single inhibition site or a single class of inhibition site.

2.6. Fluorescence spectra studies

2.6.1. Fluorescence quenching spectra

The fluorescence quenching assay was analyzed at three different temperatures (298, 304 and 310 K) with an excitation wavelength of 280 nm and emission wavelength from 300 to 500 nm. The excitation and emission slit widths were set at 5.0 nm. Various concentrations of SAC (from 0 to 19.61 μM) were successively added into 3.5 mL of XO solution (0.1 U/mL). All the mixtures were balanced for 10 min before measurements. Appropriate blanks corresponding to the PB solution were subtracted to correct the background fluorescence intensity.

In order to eliminate the effect of UV–vis absorption of SAC on the recorded fluorescence intensity, all the fluorescence intensities for absorption of excitation and emitted light were corrected using the Eq. (5) [27]:

$$F_c = F_m e^{\frac{A1+A2}{2}} \quad (5)$$

where F_c and F_m are the corrected and measured fluorescence intensities, respectively. A_1 and A_2 are the absorbance of inhibitor at the excitation and emission wavelengths, respectively. The corrected fluorescence intensity was used to calculate the related parameters.

To reveal the probable quenching mechanism between SAC and XO, the fluorescence quenching data were analyzed by the Stern-Volmer equation [28]:

$$\frac{F_0}{F} = 1 + K_{sv}[Q] = 1 + K_q\tau_0[Q] \quad (6)$$

where F_0 and F are the fluorescence intensities of XO before and after addition of quencher, respectively; K_{sv} is the Stern-Volmer quenching constant ($K_{sv} = K_q\tau_0$), which is determined by linear regression of a plot of F_0/F vs. [Q]; K_q is the biomolecule quenching rate constant; τ_0 (10^{-8} s) is the average lifetime of fluorophore without quencher; [Q] is the concentration of the quencher.

There are two types of fluorescence quenching mechanism: static (complex formation) and dynamic (collisional process). To confirm the type of fluorescence quenching mechanism, a double logarithmic equation was depicted to analyze binding constant (K) and number of binding site (n) at different temperatures by the Eq. (7) [29]:

$$\lg\frac{F_0 - F}{F} = \lg K + n\lg[Q] \quad (7)$$

where F_0 and F are the fluorescence intensities of XO treated without or with the quencher, respectively; [Q] is the concentration of the quencher.

To further characterize the intermolecular forces between SAC and XO, thermodynamic parameters were calculated through the van't Hoff equation [30]:

$$\lg K = -\frac{\Delta H^\circ}{2.303RT} + \frac{\Delta S^\circ}{2.303R} \quad (8)$$

where ΔH^o and ΔS^o are enthalpy change and entropy change, respectively. If the temperature does not change distinctly, both values can be regarded as constant. R (8.314 J mol^{-1} K^{-1}) is gas constant; T is the absolute temperature 298, 304 and 310 K. Thus, the value of free energy change (ΔG^o) can be obtained by the Eq. (9):

$$\Delta G^\circ = \Delta H^\circ - T\Delta S^\circ \quad (9)$$

2.6.2. The synchronous fluorescence spectra

The synchronous fluorescence spectra were recorded by setting the excitation and emission wavelength interval (Δλ) at 15 and 60 nm over a wavelength of 200–500 nm, at which the spectrum only monitored the spectroscopic behavior of residues tyrosine (Tyr) and tryptophan (Trp) of protein, respectively. In addition, the ratio of synchronous fluorescence quenching (RSFQ) is calculated through the Eq. (10):

$$\text{RSFQ}(\%) = 1 - \frac{F}{F_0} \quad (10)$$

where F_0 and F are the fluorescence intensities of XO without and with SAC, respectively.

2.6.3. ANS-binding fluorescence probe experiment

ANS-binding fluorescence assay was carried out by the modified methods [31]. The probe ANS (final concentration of 5 μM) was pre-incubated with 0.1 U/mL of XO for one hour, and then the solution was added to the quartz cuvette. Various concentrations of SAC (from 0 to 19.61 μM) were successively added to the mixture solution. All the mixtures were balanced for 10 min before measurements. The excitation wavelength was set at 380 nm and the emission wavelength was set from 400 to 650 nm. Excitation and emission slit widths were set at 5 nm.

2.7. FT-IR spectra

The spectra were monitored using the ATR method over the spectral range of 1800–1400 cm^{-1} with the resolution of 4 cm^{-1} and 60 scans. XO solutions without or with SAC were evenly coated on the ZnSe chip. The spectra of free SAC and the SAC-XO mixture solution (10 μM and 0.1 U/mL, respectively) were measured based on the collected background spectrum as interferogram. The spectral subtraction of free SAC from SAC-XO mixture was completed under the same assay conditions. The collected spectra were depicted by baseline subtraction, smoothing, second derivative spectrum, deconvolution and curve-fitted of spectrum, which was analyzed on PeakFit v4.04 (AISN software Inc.).

2.8. CD spectra

CD measurements were recorded on CD spectrometer with wavelength from 200 to 250 nm and a scan speed of 100 nm min^{-1} under constant nitrogen flush at room temperature. The concentration of XO was maintained at 0.1 U/mL, and the molar ratios of SAC to XO were set as 0:1, 5:1, 10:1 and 20:1, respectively. The spectral subtraction of PB solution from SAC-XO mixture was completed under the same assay conditions. The corresponding contents of different secondary structures of XO were analyzed by the online SELCON3 program (http://dichroweb.cryst.bbk.ac.uk/html/home.shtml).

2.9. Molecular docking

Molecular docking was performed on AutoDock v4.2. The X-ray co-crystal structure of XO/salicylic acid complex from bovine milk (PDB code: 1FIQ) was obtained from RCSB Protein Database Bank. The 3D structures of small molecules were generated by Chem3D Ultra 8.0 and the energy minimizations were carried out by SYBYL X-2.0. The rotatable bonds of ligands were detected and assigned with AutoDock tools. The protein was prepared by repairing the missing and terminal residues of polypeptide chains, deleting waters, assigning atom types and adding hydrogen atoms. The size of the grid box was set as 60 × 60 × 60 Å with a grid spacing 0.375 Å to enclose the active site of XO. Docking calculations were performed by the Lamarckian genetic algorithm (LGA) with run times of 100. All the other miscellaneous parameters were set as default. Results differing by ≤ 2 Å in a positional root mean-square deviation (RMSD) were clustered together. The docked model with the lowest binding energy and highest percentage frequency was chosen to represent the most favorable binding mode as predicted by the program. The output from AutoDock was rendered with PyMOL to give graphic display.

3. Results and discussion

3.1. XO inhibitory activity in vitro

The inhibitory activity of SAC on XO with various concentrations was evaluated *in vitro*. As shown in Fig. 2A, it was found that SAC exhibited considerable inhibition rates against XO in a concentration-dependent manner compared to allopurinol (positive control). The IC_{50} values (loss of 50% enzymatic activity) of compounds SAC and allopurinol were determined as 5.84 ± 0.18 and 2.90 ± 0.12 μM, respectively. These results suggested that SAC may be an effective XO inhibitor due to the strong inhibitory potency. In our previous study [32], it was found that SAC exhibited more potent XO inhibitory activity in a mixed competitive manner, while compounds salvianolic acid A and isosalvianolic acid C showed weak inhibition activity, which was in accordance with the present results. Also, the synthetic compound **4a** with the core scaffold 2-arylbenzo[*b*]furan (SAC derivative) was reported as a novel XO inhibitor [25]. All the results described above indicated that 2-arylbenzo[*b*]furan ring played an important role in the inhibition effect of XO, which was further confirmed by the following molecular docking analysis and was consistent with the structure-activity relationship of our previous studies [25].

To corroborate the reversibility of SAC-mediated inhibition, the kinetic plots of v vs. [XO] at various concentrations of the inhibitor were depicted. As shown in Fig. 2B, all the straight lines passed through the origin point and a decrease tendency in the slope of the lines came with the increasing concentrations of the inhibitor, indicating that the inhibition of SAC on XO was reversible.

3.2. Type of inhibition by Lineweaver-Burk plots analysis

Kinetic mechanism of SAC-mediated inhibition was evaluated by double-reciprocal Lineweaver-Burk plots (Fig. 3A). It showed that all the data lines intersected in the second quadrant on the Lineweaver-Burk plots. The values of horizontal axis intercept ($-1/K_m$) and vertical axis intercept ($1/V_{max}$) both enhanced with the increasing amount of inhibitor, suggesting that the inhibition of SAC belonged to the mixed-type competitive manner. From the secondary plots of Lineweaver-Burk curves, K_i and K_{is} were calculated to be 6.13 and 17.63 μM, respectively. The K_i value was smaller (approximately equal to 3-fold) than K_{is}, which indicated that SAC tended to be easily and firmly bound to the free XO rather than xanthine-XO complex. Additionally, the second plots of slope and Y-intercept versus the concentration of the inhibitors (Fig. 3B) were all linearly fitted, demonstrating that SAC had a single or a class of binding site on the enzyme.

3.3. Inactivation kinetics of XO in the presence of SAC

The time-course measurement of XO activity mediated by SAC was carried out to explore enzyme inactivation kinetics. The different

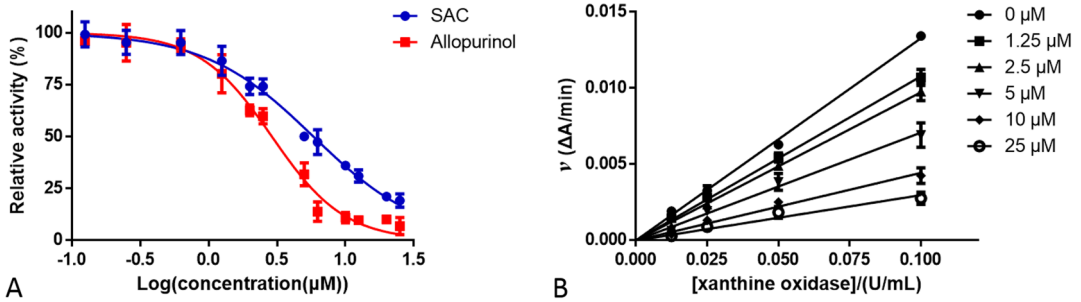

Fig. 2. (A) Inhibitory effects of compounds SAC and allopurinol on XO. Each point indicates the average ± S.D. of triplicate measurements. (B) Plots of v vs. [XO]. The concentrations of compound SAC were set as 0, 1.25, 2.5, 5, 10 and 25 μM, respectively.

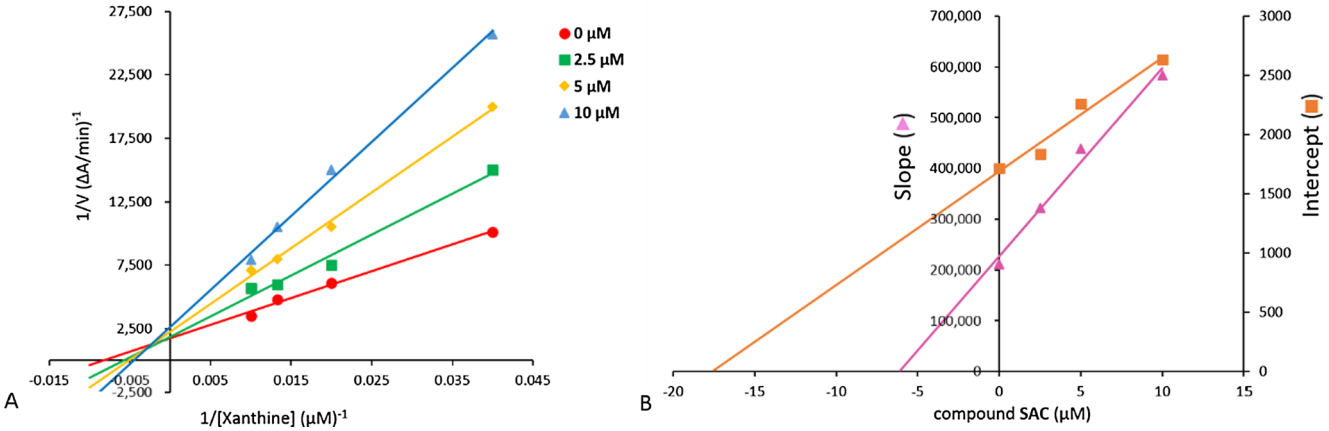

Fig. 3. Steady-state kinetic analysis of XO by compound SAC. (A) Lineweaver-Burk plots in the absence of SAC or at the different concentrations of SAC. (B) Inset, K_i and K_{is} values were obtained from secondary plots of the slopes of the Lineweaver-Burk plots and the apparent $1/V_{max}$ versus the inhibitor concentrations, respectively. Each point indicates the average value from three independent experiments.

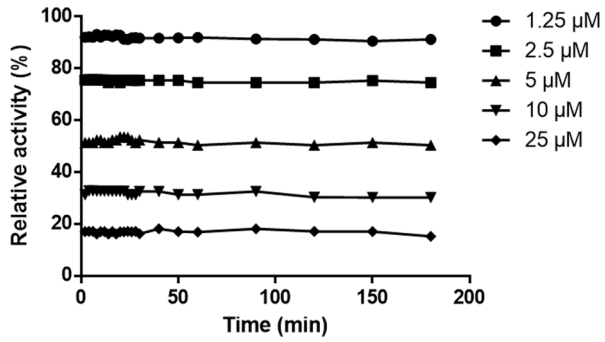

Fig. 4. Kinetic time-courses for relative activity of XO in the presence of SAC (pH = 7.0, T = 310 K) at the concentrations of 1.25, 2.5, 5, 10 and 25 μM, respectively. Aliquots were collected at the indicated time intervals, respectively. The final concentrations of XO and the substrate were 0.02 U/mL and 0.12 mM, respectively.

concentrations of SAC were prepared at 1.25, 2.5, 5, 10 and 25 μM, respectively. And the final concentrations of XO and xanthine were determined as 0.02 U/mL and 0.12 mM, respectively. As shown in Fig. 4, the XO activity did not present significant changes and maintained at relatively constant values with the increasing time under different concentrations of SAC. When the concentration of SAC was 1.25 μM, the relative activity of XO was approximately equal to 90% compared to the activity of native state. Also, the enzyme activity remained about 17% during the measured process (0–180 min) when the maximum test concentration of SAC was set as 25 μM. These data were consistent with the analytical results shown in Fig. 2A. In a very short time (less than 30 s), which was not able to monitor effectively under the assay conditions, most of the XO activity was rapidly abolished. And the rest of the enzyme activity was then kept at a relatively constant level under the monitor of 180 min. The obtained results suggested that SAC could easily bind to the active site and mediate the rapid inactivation process of the enzyme.

3.4. Fluorescence quenching studies of XO induced by SAC

SAC showed remarkable inhibitory activity on XO, indicating that SAC may directly bind to the enzyme. However, the detailed interaction mechanism was still ambiguous. In order to further explore the proposed interaction mode between SAC and XO, the fluorescence assay was performed to provide more information on the interaction process, such as binding mechanism, binding constant and binding site.

XO contains three kinds of light-emitting groups, namely, tryptophan, tyrosine and phenylalanine. Herein, the fluorescence quenching assay was performed to obtain information on the interaction of SAC with XO. As shown in Fig. 5A, two fluorescence emission peaks could be observed at 340 and 405 nm, while SAC (curve m) did not exhibit intrinsic fluorescence under the assay conditions. The change of fluorescence intensity at 340 nm was more distinct than that of 405 nm. Therefore, we focused on the fluorescence emission peak at 340 nm. When the concentration of SAC from 0 to 19.61 μM, the fluorescence intensity (curves from a to k) at 340 nm decreased remarkably by 70.2% and the maximum emission wavelength did not show any obvious shift. These results proved that SAC could interact with the enzyme and effectively quench its intrinsic fluorescence.

The obtained Stern-Volmer plots for the quenching of XO by SAC at three different temperatures (298, 304 and 310 K) exhibited a good linearity (Fig. 5B), indicating that the fluorescence quenching type was a single quenching mechanism either static or dynamic quenching. Further result listed in Table 1 presented that K_{sv} values gradually decreased with the increasing temperatures. The corresponding K_q values were determined as $(1.04 \pm 0.06) \times 10^{13}$, $(0.67 \pm 0.13) \times 10^{13}$ and $(0.49 \pm 0.02) \times 10^{13}$ L mol^{-1} s^{-1} at 298, 304 and 310 K, respectively, which were much larger than the maximum diffusion collision quenching constant (2.0×10^{10} L mol^{-1} s^{-1}) [33]. These results demonstrated that the static quenching might play a predominant role in the fluorescence quenching process and the quenching was thus probably initiated by the formation of SAC-XO complex.

Furthermore, as shown in Table 1, the remarkably increased trend of K values with the rising temperature was observed, indicating that the binding capacity of SAC to XO gradually improved and the binding effect belonged to an endothermic and entropy-driven reaction process. The n values were all approximately equal to 1 at different temperatures, which suggested that SAC bound to a class of binding site on XO, which was in accordance with the analysis of the Lineweaver-Burk plots.

3.5. Thermodynamic analysis

Determination of thermodynamic parameters of binding reaction is beneficial to confirm the acting forces, which mainly include hydrophobic force, electrostatic interaction, van der Waals force and hydrogen bonds. As shown in Table 1, the negative value of ΔG^o showed that the interaction between XO and SAC occurred spontaneously. The positive values of ΔH^o (224.76 ± 0.14 kJ mol^{-1}) and ΔS^o (838.23 ± 0.15 J mol^{-1} K^{-1}) demonstrated that the binding process was predominately driven by the hydrophobic interactions [34]. The obtained interaction process was similar to the reported XO inhibitor

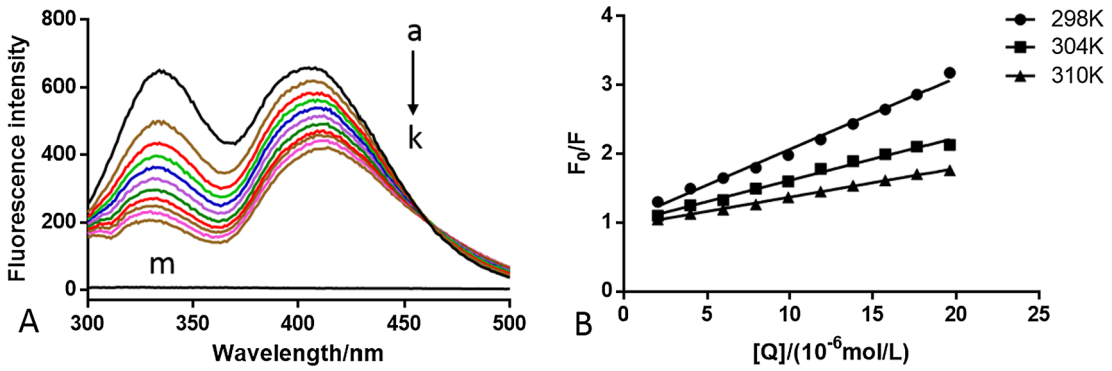

Fig. 5. (A) Fluorescence spectra of XO in the presence of SAC at different concentrations (pH = 7.0, T = 298 K, λex = 280 nm, λem = 340 nm). c(XO) = 0.1 U/mL, and c(SAC) = 0, 2, 3.98, 5.96, 7.94, 9.9, 11.86, 13.81, 15.75, 17.68, 19.61 μM for curves a → k, respectively. Curve m shows the emission spectrum of SAC only, c (SAC) = 5 μM. (B) The Stern-Volmer plots for the fluorescence quenching at different temperatures (298, 304 and 310 K).

luteolin [35]. However, hydrogen binding should not be ignored because the experimental system was in aqueous solution and many hydroxyl groups existed on the chemical structure of SAC, which was further confirmed by molecular docking.

3.6. Synchronous fluorescence spectroscopy

Synchronous fluorescence spectroscopy has emerged as an ideal tool to observe conformational changes in proteins, and used to measure the fluorescence quenching and the possible shift of the maximum emission wavelength, which is correlated with the alteration of the polarity around the chromophore (tyrosine and tryptophan) microenvironment. It is well known that the assay on synchronous fluorescence of XO will provide the characteristic information for residues Tyr and Trp when the wavelength interval (Δλ) is fixed at 15 and 60 nm, respectively.

The synchronous fluorescence spectra of interaction between SAC and XO were presented in Fig. 6. It was shown that the fluorescence intensity of XO decreased regularly along with the addition of SAC, which further demonstrated the occurrence of fluorescence quenching during the binding process. Moreover, the maximum emission wavelength of the residue Trp shifted from 291 to 284 nm (Fig. 6A), while the synchronous fluorescence spectrum of Tyr residue did not change significantly at 285 nm (Fig. 6B). This phenomenon demonstrated that the enzyme microenvironment changed, the surrounding polarity of residue Trp decreased and the hydrophobicity increased, resulting in the conformational changes of XO, which further proved that the hydrophobic interaction was present in the interaction of SAC with XO [36]. The microenvironment of Tyr residue exhibited no obvious change when SAC binding to XO. In addition, the RSFQ values of residues Tyr and Trp were calculated (Fig. 6C). The RSFQ value of Tyr was distinctly higher than that of Trp under the same assay conditions. These results indicated that the residue Tyr may have a better contribution to the fluorescence quenching effect of XO, and compound SAC was closed to Tyr but not to Trp in the active site of the enzyme.

3.7. ANS-binding fluorescence probe experiment

ANS serves as a comprehensive fluorescence probe for the study of hydrophobic regions of proteins [37]. The fluorescence of ANS is very weak, while it will be distinctly increased as it enters the hydrophobic region of the enzyme and interacts with the enzyme. Herein, ANS-binding fluorescence probe assay was conducted to confirm the change of the hydrophobic domain of XO mediated by SAC. The fluorescence intensity of XO labeled by ANS (curve b) was higher than that of the blank ANS (curve a), and it was gradually enhanced with the addition of SAC (curve b–l) (Fig. 7A). This could be ascribed to the fact that SAC bound to the enzyme after being added to the enzyme-ANS system, which resulted in the hydrophobic region being opened further. This interaction greatly accelerated the ANS activity interacting with the hydrophobic surface of XO, which effectively improved the fluorescence intensity of ANS. The similar observations were also maintained for the interaction between benzaldehyde thiosemicarbazide compounds and XO based on the ANS-binding fluorescence probe method [31].

In addition, from Fig. 7B, the fluorescence peak area was gradually increased, and the maximum peak wavelength firstly decreased and then kept at a relatively constant level with the addition of SAC. Hydrophobic surface change is related to conformation change of the active site as well as the whole enzyme. Thus, these results of ANS-binding fluorescence assay provided some evidences on the conformational state of XO mediated by SAC, which led to local exposure of the hydrophobic region, even at non-saturated concentrations [31]. This conclusion is highly consistent with the results of enzyme kinetics assay and fluorescence quenching assay. Moreover, hydrophobic interactions play a key role in the interaction of SAC with XO.

3.8. FT-IR spectra of XO mediated by SAC

FT-IR spectrum is an effective and popular technique to determine the secondary structures of protein. There are nine characteristic vibrational bands or group frequencies for proteins, which are sensitive to

Table 1
The quenching constant (K_{SV}), binding constant (K), number of binding site (n) and corresponding thermodynamic parameters for the interaction between SAC and XO. Data were measured as the average ± S.D. of triplicate measurements.

T (K)	K_{SV} ($\times 10^5$ L mol^{-1})	R^a	K ($\times 10^5$ L mol^{-1})	n	R^b	ΔH^o (kJ mol^{-1})	ΔG^o (kJ mol^{-1})	ΔS^o (J mol^{-1} K^{-1})
298	1.04 ± 0.06	0.9905	0.21 ± 0.09	0.8585 ± 0.03	0.9847	224.76 ± 0.14	−25.03 ± 0.07	838.23 ± 0.15
304	0.67 ± 0.13	0.9946	1.91 ± 0.14	1.0976 ± 0.07	0.9953		−30.06 ± 0.04	
310	0.49 ± 0.02	0.9907	7.09 ± 0.12	1.2542 ± 0.02	0.9978		−35.09 ± 0.11	

[a] R is the correlation coefficient for the Ksv values.
[b] R is the correlation coefficient for the K values.

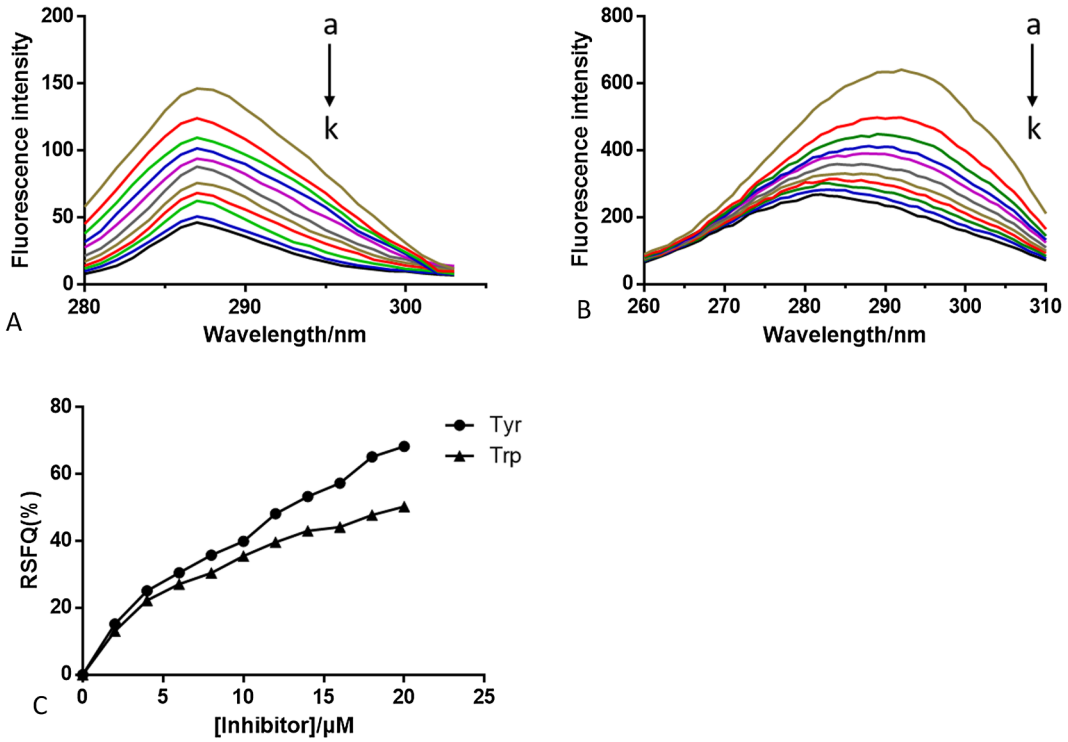

Fig. 6. The synchronous fluorescence spectra of XO in the absence and presence of SAC (A) $\Delta\lambda$ = 15 nm, (B) $\Delta\lambda$ = 60 nm and the RSFQ value of compound SAC on XO (pH = 7.0, T = 298 K). c(XO) = 0.1 U/mL, and c(SAC) = 0, 2, 3.98, 5.96, 7.94, 9.9, 11.86, 13.81, 15.75, 17.68, 19.61 μM for curves a → k, respectively.

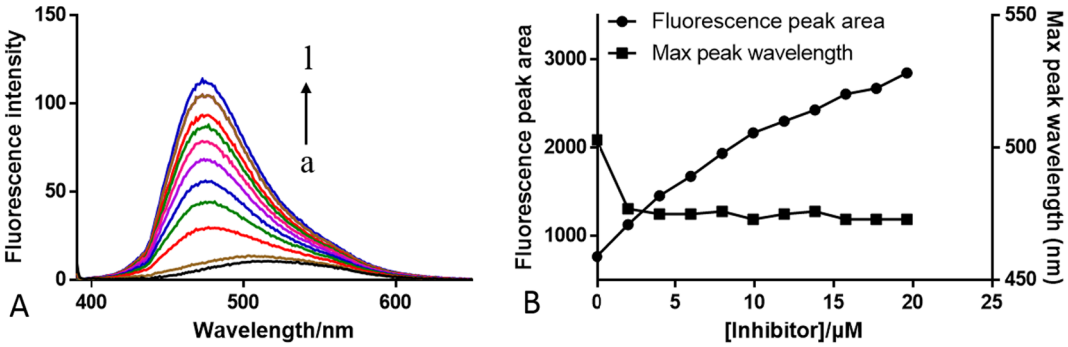

Fig. 7. (A) ANS fluorescence probe spectra of XO in the absence and presence of SAC at various concentrations (pH = 7.0, T = 298 K). (B) The fluorescence peak areas and maximum peak wavelengths of XO-SAC complex at different concentrations of SAC. Curve a is for the blank ANS, and curves b → l are the concentrations of SAC at 0, 2, 3.98, 5.96, 7.94, 9.9, 11.86, 13.81, 15.75, 17.68, 19.61 μM, respectively.

the conformational changes of protein secondary structure and are largely constrained to group frequency interpretations [38]. Among them, amide I band (1700–1600 cm^{-1}, mainly C=O stretching vibration) and amide II band (1600–1500 cm^{-1}, C–N stretching coupled with N–H in-plane bending) are main vibrational bands of the peptide moiety related to the secondary structures of proteins [39]. As shown in Fig. 8A, the peak position of amide I band of XO moved from 1645 to 1649 cm^{-1} with the addition of SAC, whereas that of amide II band shifted to a lesser extent (from 1548 to 1545 cm^{-1}). The similar phenomenon was also observed for the FT-IR spectrum changes of XO induced by galangin [30].

Generally, amide I band is more widely used to investigate protein secondary structures because of its high sensitive. The spectral ranges of 1615–1637 cm^{-1}, 1638–1648 cm^{-1}, 1649–1660 cm^{-1}, 1661–1680 cm^{-1} and 1681–1692 cm^{-1} are commonly assigned to β-sheet, random coil, α-helix, β-turn and β-antiparallel, respectively [40]. As shown in Table 2, compared to the contents of each secondary structure without SAC, the contents of α-helix and β-antiparallel increased from 11.17% to 13.60% and from 5.69% to 10.18% respectively, while the contents of β-sheet, β-turn and random coil decreased from 40.74% to 37.76%, 17.62% to 15.92%, and from 24.78% to 22.55% respectively, after adding SAC (Fig. 8C and D). These changes illustrated that SAC interacted with the C=O and C–N groups of XO structure and induced the rearrangement of the carbonyl hydrogen bonding pattern of polypeptide.

3.9. Secondary structure analysis of CD spectra

CD spectrum has emerged as a useful means to characterize the secondary structure of protein. As shown in Fig. 8B, the far-UV CD spectra of XO with varied concentration of SAC were recorded mainly by only one negative band at 216 nm (feature of β-Sheet) for the peptide bonds of the β-Sheet. Conformational transition of XO could be monitored by changes in position and intensity of the bands in CD

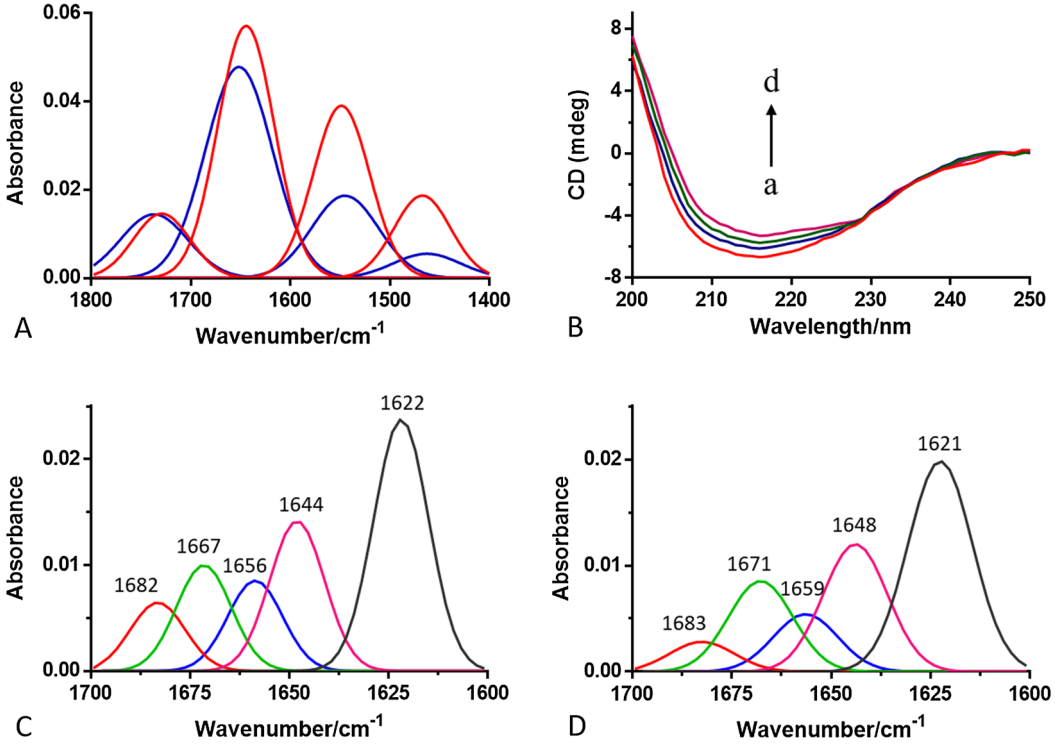

Fig. 8. (A) The FT-IR spectra of free XO (colored as red curve) and difference spectra [(SAC-XO solution)-SAC solution] (colored as blue curve) in the region of 1800–1400 cm^{-1} at pH 7.0 and room temperature. *c*(XO) = 0.1 U/mL and *c*(SAC) = 10 μM. (B) CD spectra of XO-SAC system in the presence of increasing amounts of SAC at pH 7.0 and room temperature. *c*(XO) = 0.1 U/mL, and *c*(SAC) = 0, 5, 10 and 20 μM for curves a → d, respectively. The curve-fitted amide I band of free XO (C) and its SAC complex (D).

Table 2
The contents (FT-IR spectra) of different secondary structures of free XO and XO-SAC complex at pH 7.0 and room temperature.

Concentration of SAC (μM)	α-Helix (%)	β-Sheet (%)	β-Turn (%)	Random coil (%)	β-Antiparallel (%)
0	11.17	40.74	17.62	24.78	5.69
10	13.60	37.76	15.92	22.55	10.18

Table 3
The contents (CD spectra) of different secondary structures of free XO and XO-SAC complex at pH 7.0 and room temperature.

Molar ratio of [SAC]:[XO]	α-Helix (%)	β-Sheet (%)	β-Turn (%)	Random coil (%)
0:1	7.93	42.05	22.30	27.72
5:1	9.72	41.17	22.04	27.07
10:1	11.64	40.35	21.77	26.24
20:1	14.87	39.72	21.25	24.16

spectrum. With the addition of SAC, the CD intensity was decreased obviously without any significant changes in the peak position and shape. Moreover, the proportion of different secondary structures of XO was calculated by the online SELCON3 program (see Table 3). With the increasing amounts of SAC, the proportion of α-helix increased from 7.93% to 14.87%, whereas the contents of β-sheet, β-turn and random coil decreased from 42.05% to 39.72%, 22.30% to 21.25% and 27.72% to 24.16%, respectively. These results proved that SAC could induce the rearrangement and conformational changes of the enzyme and then prevent the entrance of substrate, which contributed to its potent XO inhibitory activity. SAC-induced secondary structure changes of the enzyme were similar to other XO inhibitors. For example, the natural flavonoids luteolin [35] and galangin [30] were also reported to significantly decrease the β-sheet content of the enzyme and induce the secondary structure rearrangement.

3.10. Molecular docking studies

Molecular docking is commonly used to predict the visible binding modes of ligand-protein complexes. Firstly, the original ligand salicylic acid was re-docked into XO and a RMSD value of 0.42 Å yielded. As shown in Fig. 9A, cluster analysis of 100 docking runs displayed a total of 29 multimember conformational clusters at a RMSD tolerance of 2.0 Å. The cluster with the lowest energy and the most frequent locus (red histogram) was chosen to the binding orientation analysis. It was found that SAC inserted into the activity cavity, where the active site with Mo-pt domain locates (Fig. 9C). Compound SAC was adjacent to some hydrophobic residues (Leu648, Phe914, Phe1009, Val1011, Phe1013 and Pro1076) in the active pocket of XO, indicating that the presence of hydrophobic interactions between SAC and XO. Moreover, there were four hydrogen bonds formed between the free hydroxyl groups of SAC and residues Arg880, Thr1010, Ser1082 of XO, and potential aromatic interaction (π-π effects) was also observed due to the two key residues (Phe914 and Phe1009) around the protein (Fig. 9D). The predicted driving force of SAC-XO interaction was hydrophobic interactions and hydrogen bonds, which was consistent with the analysis of fluorescence spectra.

Based on the docking results, it may be inferred that SAC could compete with the substrate xanthine to bind the active site of XO. If the concentration of SAC was low, the formation of the reaction product uric acid may be slightly inhibited. With the increasing concentration of SAC, it could remarkably induce the secondary structure changes of the enzyme, prevent the entrance of the substrate and then strongly inhibit the formation of uric acid. This supposition was in accordance with the experimental results (especially of FT-IR and CD spectra), both of which provided intuitive data to understand the principal inhibition mechanism of SAC against XO.

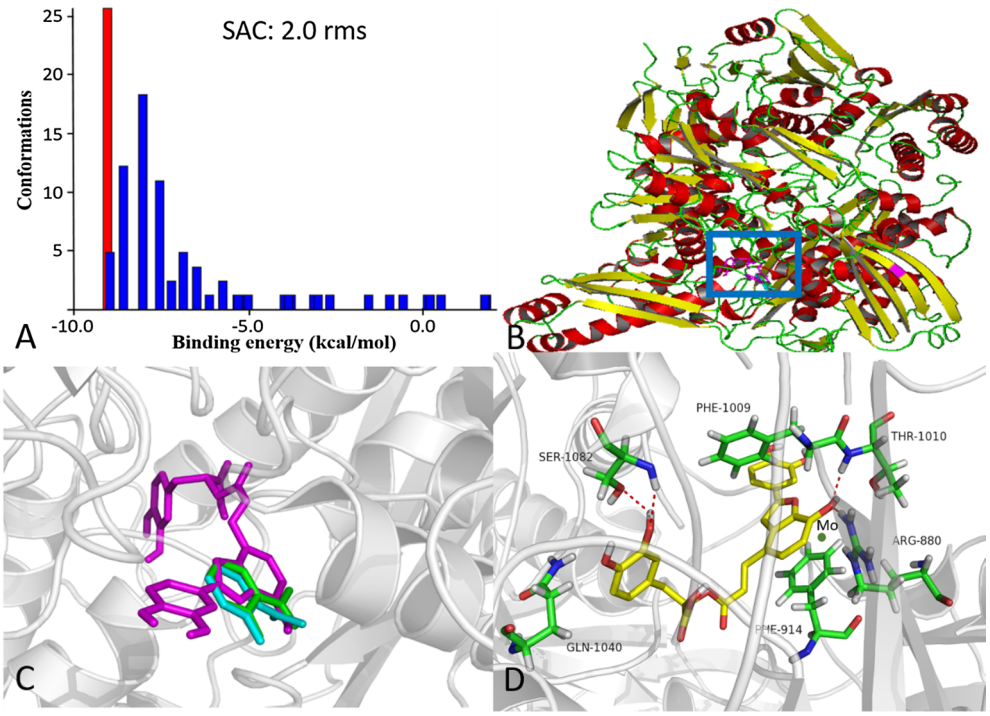

Fig. 9. (A) Cluster analysis of the docking runs of SAC with XO (PDB code: 1FIQ). (B) Molecular docking results of the inhibitors SAC and salicylic acid binding to XO. (C) View of superimposed docking conformations for the inhibitors binding to the active pocket of XO. The original ligand salicylic acid is colored as green, the re-docked ligand is colored as cyan, and the magenta represents compound SAC. (D) A close-up view of compound SAC bound in the active site of XO. The structure of compound SAC are colored as yellow. Key residues are shown as stick models and hydrogen bonds are labeled as red dashed lines.

4. Conclusions

In this study, multi-spectroscopy methods including enzyme kinetics, fluorescence spectrum, FT-IR, CD spectrum and molecular docking have been used to clarify the interaction between SAC and XO. As a result, SAC exhibited a significant inhibitory activity on XO with IC_{50} value of 5.84 ± 0.18 μM. It reversibly inhibited the enzyme in a mixed-type manner with K_i and K_{is} values of 6.13 and 17.63 μM, respectively. The activity of XO was rapidly inactivated by SAC through the first-order kinetics process. The fluorescence chromophore was quenched by SAC in a static quenching mechanism due to the formation of XO-SAC complex. The calculated thermodynamic parameters indicated that their binding was spontaneous and was dominated mainly by hydrophobic interaction. Moreover, the analysis of synchronous fluorescence, FT-IR and CD spectra revealed that SAC bound to the active site and induce the rearrangement and secondary structure changes of XO, which was further confirmed by molecular docking. Therefore, the natural product SAC could effectively inhibit XO activity by spontaneously binding to the enzyme, occupying the catalytic center (Mo-pt domain), preventing the entrance of substrate and inducing the conformational changes of secondary structures of XO, which further affected the tertiary structure of the enzyme. Overall, such findings not only put insight into understanding the proposed binding mechanism of SAC to XO but also provide some valuable information for us to design novel XO inhibitors taking SAC as drug leads in future.

Acknowledgments

This work was financially supported by the Natural Science Foundation of Anhui Province (No. 1908085QH346), the Introduction of Talent Research Start-up Fund of Anhui Polytechnic University (No. 2017YQQ017) and the Pre-research project of National Natural Science Foundation of China of Anhui Polytechnic University (No. 2019yyzr10).

Conflicts of interest

The authors declare that there is no conflict of the interest.

Appendix A. Supplementary material

Supplementary data to this article can be found online at https://doi.org/10.1016/j.bioorg.2019.102981.

References

[1] A.M. Abeles, J.Y. Park, M.H. Pillinger, B.N. Cronstein, Update on gout: pathophysiology and potential treatments, Curr. Pain. Headache Rep. 11 (2007) 440–446.
[2] C. Enroth, B.T. Eger, K. Okamoto, T. Nishino, E.F. Pai, Crystal structures of bovine milk xanthine dehydrogenase and xanthine oxidase: structure-based mechanism of conversion, Proc. Natl. Acad. Sci. 97 (2000) 10723–10728.
[3] R. Harrison, Structure and function of xanthine oxidoreductase: where are we now? Free Radical Biol. Med. 33 (2002) 774–797.
[4] D. Kumar, G. Kaur, A. Negi, S. Kumar, S. Singh, R. Kumar, Synthesis and xanthine oxidase inhibitory activity of 5,6-dihydropyrazolo/pyrazolo[1,5-c] quinazoline derivatives, Bioorg. Chem. 57 (2014) 57–64.
[5] J.H. Cheng, A.M. Huang, T.C. Hour, S.C. Yang, Y.S. Pu, C.N. Lin, Antioxidant xanthone derivatives induce cell cycle arrest and apoptosis and enhance cell death induced by cisplatin in NTUB1 cells associated with ROS, Eur. J. Med. Chem. 46 (2011) 1222–1231.
[6] S. Khanna, S. Burudkar, K. Bajaj, P. Shah, A. Keche, U. Ghosh, Isocytosine-based inhibitors of xanthine oxidase: design, synthesis, SAR, PK and *in vivo* efficacy in rat model of hyperuricemia, Bioorg. Med. Chem. Lett. 22 (2012) 7543–7546.
[7] C. B-Rao, A. Kulkarni-Almeida, K.V. Katkar, S. Khanna, U. Ghosh, A. Keche, Identification of novel isocytosine derivatives as xanthine oxidase inhibitors from a set of virtual screening hits, Bioorg. Med. Chem. 20 (2012) 2930–2939.
[8] S.J. Wang, J.F. Yan, J. Wang, J.R. Chen, T.J. Zhang, Y. Zhao, Synthesis of some 5-phenylisoxazole-3-carboxylic acid derivatives as potent xanthine oxidase inhibitors, Eur. J Med. Chem. 45 (2010) 2663–2670.
[9] J. Li, F.P. Wu, X.G. Liu, Y.K. Zou, H.X. Chen, Z. Li, Synthesis and bioevaluation of 1-phenyl-pyrazole-4-carboxylic acid derivatives as potent xanthine oxidoreductase inhibitors, Eur. J. Med. Chem. 140 (2017) 20–30.
[10] H.J. Tang, L. Yang, J.H. Li, J. Chen, Molecular modelling studies of 3,5-dipyridyl-1,2,4-triazole derivatives as xanthine oxidoreductase inhibitors using 3D-QSAR, Topomer CoMFA, molecular docking and molecular dynamic simulations, J. Taiwan Inst. Chem. E 68 (2016) 64–73.
[11] K. Matsumoto, K. Okamoto, N. Ashizawa, T. Nishino, FYX-051: a novel and potent hybrid-type inhibitor of xanthine oxidoreductase, J. Pharmacol. Exp. Ther. 336 (2010) 95–103.
[12] S. Ishibuchi, H. Morimoto, T. Oe, T. Ikebe, H. Inoue, A. Fukunari, Synthesis and structure-activity relationships of 1-phenylpyrazoles as xanthine oxidase inhibitors, Bioorg. Med. Chem. Lett. 11 (2001) 879–882.
[13] Q. Guan, Z. Cheng, X. Ma, L. Wang, D. Feng, Y. Cui, K. Bao, L. Wu, W. Zhang, Synthesis and bioevaluation of 2-phenyl-4-methyl-1,3-selenazole-5-carboxylic acids as potent xanthine oxidase inhibitors, Eur. J. Med. Chem. 85 (2014) 508–516.
[14] S. Chen, T. Zhang, J. Wang, F. Wang, H. Niu, C. Wu, S. Wang, Synthesis and

evaluation of 1-hydroxy/methoxy-4-methyl-2-phenyl-1*H*-imidazole-carboxylic acid derivatives as non-purine xanthine oxidase inhibitors, Eur. J. Med. Chem. 103 (2015) 343–353.
[15] K.C. Morrison, P.J. Hergenrother, Natural products as starting points for the synthesis of complex and diverse compounds, Nat. Prod. Rep. 31 (2014) 6–14.
[16] D.A. Dias, S. Urban, U. Roessner, A historical overview of natural products in drug discovery, Metabolites 2 (2012) 303–336.
[17] L. Ouyang, Y. Luo, M. Tian, S.Y. Zhang, R. Lu, J.H. Wang, Plant natural products: from traditional compounds to new emerging drugs in cancer therapy, Cell Proliferat. 47 (2014) 506–515.
[18] S.F. Tsai, S.S. Lee, Neolignans as xanthine oxidase inhibitors from *Hyptis rhomboids*, Phytochemistry 101 (2014) 121–127.
[19] H.X. Liu, M.T. He, H.B. Tan, W. Gu, S.X. Yang, Y.H. Wang, Xanthine oxidase inhibitors isolated from *Piper nudibaccatum*, Phytochem. Lett. 12 (2015) 133–137.
[20] K. Nepali, G. Singh, A. Turan, A. Agarwal, S. Sapra, R. Kumar, A rational approach for the design and synthesis of 1-acetyl-3,5-diaryl-4,5-dihydro(1*H*)pyrazoles as a new class of potential non-purine xanthine oxidase inhibitors, Bioorg. Med. Chem. 19 (2011) 1950–1958.
[21] S.M. Darwish, S.A. Makharza, M.M. Abu-Hadid, S.A. Makharza, M.M. Abu-Hadid, Spectroscopic investigations of pentobarbital interaction with human serum albumin, J. Mol. Struct. 963 (2010) 122–129.
[22] G.W. Zhang, Y.D. Ma, L. Wang, Y.P. Zhang, J. Zhou, Multispectroscopic studies on the interaction of maltol, a food additive, with bovine serum albumin, Food Chem. 133 (2012) 264–270.
[23] A.S. Ghasemi, F. Mashhadban, S.M. Hoseini-Alfatemi, J. Sharifi-Rad, Conformational stability, spectroscopic and computational studies, hikes' occupied molecular orbital, lowest unoccupied molecular orbital, natural bond orbital analysis and thermodynamic parameters of anticancer drug on nanotube-A review, Cell Mol. Biol. 61 (2015) 74–78.
[24] Y. Zou, Z.Y. Qian, Y.J. Chen, H.S. Qian, G.H. Wei, Q.W. Zhang, Norepinephrine inhibits Alzheimer's amyloid-beta peptide aggregation and destabilizes amyloid-beta protofibrils: a molecular dynamics simulation study, ACS Chem. Neurosci. 10 (2019) 1585–1594.
[25] H.J. Tang, X.W. Zhang, L. Yang, W. Li, J.H. Li, J.X. Wang, J. Chen, Synthesis and evaluation of xanthine oxidase inhibitory and antioxidant activities of 2-arylbenzo [*b*]furan derivatives based on salvianolic acid C, Eur. J. Med. Chem. 124 (2016) 637–648.
[26] Z.Q. Xiong, W. Liu, L. Zhou, L.Q. Zou, J. Chen, Mushroom (*Agaricus bisporus*) polyphenoloxidase inhibited by apigenin: multi-spectroscopic analyses and computational docking simulation, Food Chem. 203 (2016) 430–439.
[27] Y.J. Wang, G.W. Zhang, J.H. Yan, D.M. Gong, Inhibitory effect of morin on tyrosinase: insights from spectroscopic and molecular docking studies, Food. Chem. 163 (2014) 226–233.
[28] W. Peng, F. Ding, Y.T. Jiang, Y. Sun, Y.K. Peng, Evaluation of the biointeraction of colorant flavazin with human serum albumin: Insights from multiple spectroscopic studies, *in silico* docking and molecular dynamics simulation, Food Funct. 5 (2014) 1203–1217.
[29] N. Shahabadi, M. Maghsudi, Z. Kiani, M. Pourfoulad, Multispectroscopic studies on the interaction of 2-tert-butylhydroquinone (TBHQ), a food additive, with bovine serum albumin, Food Chem. 124 (2011) 1063–1068.
[30] C. Zhang, G.W. Zhang, J.H. Pan, D.M. Gong, Galangin competitively inhibits xanthine oxidase by a ping-pong mechanism, Food Res. Int. 89 (2016) 152–160.
[31] M.R. Li, Y.Y. Yu, J. Liu, Z.L. Chen, S.W. Cao, Investigation of the interaction between benzaldehyde thiosemicarbazone compounds and xanthine oxidase, J Mol. Struct. 1159 (2018) 23–32.
[32] Y. Fu, H.Y. Mo, W. Gao, J.Y. Hong, J. Lu, P. Li, J. Chen, Affinity selection-based two-dimensional chromatography coupled with high-performance liquid chromatography-mass spectrometry for discovering xanthine oxidase inhibitors from *Radix Salviae Miltiorrhizae*, Anal. Bioanal. Chem. 406 (2014) 4987–4995.
[33] A. Varlan, M. Hillebrand, Spectral study of coumarin-3-carboxylic acid interaction with human and bovine serum albumins, Cent. Eur. J. Chem. 9 (2011) 624–634.
[34] P.D. Ross, S. Subramanian, Thermodynamics of protein association reactions: forces contributing to stability, Biochemistry 20 (1981) 3096–3102.
[35] J.K. Yan, G.W. Zhang, Y.T. Hu, Y.D. Ma, Effect of luteolin on xanthine oxidase: inhibition kinetics and interaction mechanism merging with docking simulation, Food Chem. 141 (2013) 3766–3773.
[36] G.W. Zhang, L. Wang, P. Fu, M.M. Hu, Mechanism and conformational studies of farrerol binding to bovine serum albumin by spectroscopic methods, Spectrochim Acta A: Mol. Biomol. Spectrosc. 82 (2011) 424–431.
[37] N. Gull, S. Chodankar, V.K. Aswal, P. Sen, R.H. Khan, Kabir-ud-Din, Spectroscopic studies on the interaction of cationic surfactants with bovine serum albumin, Colloids Surf. B 69 (2009) 122–128.
[38] Z. Ganim, A. Tokmakoff, Spectral signatures of heterogeneous protein ensembles revealed by MD simulations of 2DIR spectra, Biophys. J. 91 (2006) 2636–2646.
[39] K.M. Elkins, Rapid presumptive “fingerprinting” of body fluids and materials by ATR FT-IR spectroscopy, J. Forensic. Sci. 56 (2011) 1580–1587.
[40] G.W. Zhang, L. Wang, J.H. Pan, Probing the binding of the flavonoid diosmetin to human serum albumin by multispectroscopic techniques, J. Agric. Food Chem. 60 (2012) 2721–2729.